



# In situ processing aluminide coatings with and without tungsten carbide

Heber O. Abreu-Castillo<sup>1</sup> · Bruno P. Bueno<sup>1</sup> · Ana Sofia C. M. d'Oliveira<sup>2</sup>

Received: 9 June 2021 / Accepted: 8 September 2021 / Published online: 3 November 2021  
© The Author(s), under exclusive licence to Springer-Verlag London Ltd., part of Springer Nature 2021

## Abstract

Alloying elements have been added to  $\beta$ -NiAl to improve strength and creep resistance at high temperature enhancing  $\beta$ -NiAl attractiveness and competitiveness. Particularly, tungsten carbides (WC) have been used to modify this aluminide, resulting in an increase in hardness and improved its tribological behavior in high temperature. However, the size of WC particles and the processing conditions account for the microstructure obtained and the resulting properties. This study takes an important step toward understanding how carbide particle size can contribute or interfere in the synthesis and microstructure of NiAl-based coatings. NiAl intermetallic coatings were processed by in situ synthesis during deposition by plasma transferred arc (PTA). Powder mixtures of elementary Ni and Al powders with and without the addition of 1 wt% carbide microparticles and of 1 wt% WC nanoparticles. Carbide microparticles increased the dilution with the substrate and consequently the density of point defects, which had a strong impact on hardness. However, the addition of WC nanoparticles had a negative impact on the synthesis of NiAl, delaying/inhibiting its formation, which was reflected on the microstructure and low hardness of coatings.

**Keywords** Aluminide coatings · Plasma transferred arc · Ni aluminide tungsten carbides · Powders

## 1 Introduction

Nickel aluminides are ordered compounds that have been widely studied, especially due to the interest of the automotive (for the manufacture of pistons, valves, and turbochargers), energy (various components within gas turbines and hydroturbines), and different manufacturing industries (high-temperature molds, furnace fixtures, rollers in steel slab heating furnaces, and cutting tools) [1]. The  $\beta$ -NiAl intermetallic is particularly interesting for aerospace industry because of properties such as high melting temperature (1638 °C), chemical resistance to different environments,

fatigue performance, attractive elasticity module, together with low density ( $5.9 \text{ g.cm}^{-3}$ ) and competitive cost of raw materials [2].

Ordered phase  $\beta$ -NiAl alloys have been used in high-temperature structural applications, as single crystal for gas engine vanes or as the matrix of reinforced engine nozzle flaps, with operation temperatures above 1000 °C [3]. Because of NiAl strength and high melting temperature, it can operate at temperatures above those of Ni superalloys that are currently in use (around 1000 °C), which would allow for manufacturing more efficient engines [2]. Also, the attractive oxidation resistance, due to its capacity to rapidly form a stable and adherent protective layer of alumina ( $\text{Al}_2\text{O}_3$ ) on its surface, makes NiAl competitive to be used as coatings for protecting superalloys or as a layer in thermal barrier coatings (TBC) [4]. Those coatings are crucial for high temperature applications as they allow mechanical components to operate successfully in those environments, being protected from oxidation and also wear [3].

NiAl aluminide can be manufactured in the form of a single crystal, polycrystal, or a composite, using a variety of process, among which are powder metallurgy, casting, directional solidification [5], high pressure reaction sintering, mechanical alloying, hot isostatic pressing, and combustion

✉ Ana Sofia C. M. d'Oliveira  
sofmat@ufpr.br

Heber O. Abreu-Castillo  
heber.abreu@ufpr.br

Bruno P. Bueno  
bueno.bruno1@gmail.com

<sup>1</sup> Post-Graduation Program in Materials Engineering and Science, Universidade Federal do Paraná, Curitiba, PR, Brazil

<sup>2</sup> Mechanical Engineering Department, Universidade Federal do Paraná, Curitiba, PR, Brazil

synthesis [6]. Other methods, such as high-velocity oxygen fuel, physical vapor deposition (PVD), thermal spray, and plasma spray, are used to process NiAl aluminide coatings [7].

It has been demonstrated that NiAl aluminide has good tribological properties, which makes it an excellent material for coatings with high-temperature wear resistance, and that it can be further improved with the addition of ceramic strengthening particles [8]. Nevertheless, the high melting point of intermetallic compounds inhibit the introduction of reinforcement particles using melting procedures, which makes particularly beneficial the use of methods based on in situ synthesis to manufacture this aluminide [9].

Plasma transferred arc (PTA) is a hardfacing technique that uses powder material allowing the deposition of coatings with a sound metallurgical bonding with the substrate. Through the preparation of mixtures of powders that are injected into a plasma arc (which is formed between a tungsten electrode and the substrate), melted, and transported to the melt pool at the surface of the substrate/component, PTA can process hard, low toughness materials using in situ synthesis of compounds otherwise not possible to deposit as hardfacing coatings [7].

Due to the metallurgical bonding, PTA coating processing involves dilution with the substrate, whose elements are mixed with the powder mixture in the melt pool, having significant impacts on chemical composition and mechanical properties. Thus, aluminide coating constitution depends on the composition of powder mixtures and PTA processing parameters both impacting the dilution levels; the higher the dilution, the greater the inclusion of substrate elements, which can impact phases in coatings [10].

Previous work has shown the development of aluminide coatings by in situ synthesis of NiAl aluminide, that is, during the deposition of elemental Ni and Al powder mixtures with predefined composition, by plasma transferred arc [7]. Also, it has been reported that Fe and Cr in solid solution with NiAl impact the presence and density of point defects (vacancies or anti-sites), which strongly affect the hardness of the aluminide [11]. Furthermore, the incorporation of carbides such as WC, beyond the solubility limit of NiAl, might act as a potent precipitation strengthener, having a hardening effect and improving the tribological behavior under high temperature [8].

The size of WC particles also affects the resulting microstructure: nanoparticles might have better hardening effects than microparticles if a better distribution in the matrix is achieved [12]. However, this ideal distribution is not easy to reach because nanoparticles tend to agglomerate [13]; also, the presence of WC was shown to influence dilution and consequently the microstructure/mechanical behavior of the coatings [14]. The control of structure refinement and chemical composition fluctuation of NiAl coatings still offer opportunities in the design of coatings. This study

contributes to better tailor NiAl coating microstructure as it assesses the impact of microsize and nanosize carbides on the in situ synthesis of aluminides, during the deposition of elemental powder mixtures. A better understanding of the interaction between powders in the plasma arc will contribute to an enhanced control of the microstructure and properties of NiAl coatings.

## 2 Materials and processing

Powder mixtures were prepared containing 80 wt% Ni (crushed) and 20 wt% Al, non-spherical powders with grain size in the range from 75 to 150  $\mu\text{m}$  (Fig. 1 a and b), with and without 1 wt% tungsten carbide particles of two different sizes: WC-12 at.% Co microparticles (MPs) and WC nanoparticles (NPs) (Table 1).

Crushed MP particles were supplied with grain size within the range from 10 to 35  $\mu\text{m}$  (Fig. 1c), and NP nanoparticles with an average particle size in the range 150–200 nm and average crystalline size of 55 nm (Fig. 1d).

Elemental Ni and Al powders were homogenized in a “Y” mixer for 02 h at 12 RPM. Subsequently, drying was conducted in a furnace at 120 °C for 02 h to ensure the removal of eventual humidity in the powder. The powder mixture containing 1 wt% WC–Co microparticles (NiAl-MP mixture) followed the same procedure.

A different procedure was used to prepare the powder mixture containing 1 wt% WC nanoparticles. The reduced size of the nanoparticles results in a high surface energy and consequently a strong tendency for agglomeration, which compromises a good homogenization of powders. To mitigate agglomeration, nanoparticles were adhered to the surface of the Ni grain powders. Following procedures described by Molina-Claros et al. [13], nanoparticles were weighed and dispersed in absolute alcohol in ultrasound for 90 min. Subsequently, Ni powder was added and magnetic stirred for 90 min to improve the impregnation of the nanoparticles on the surface of the Ni grains. The mixture was put again in the ultrasound bath for another 90 min and then dried at 50 °C. Figure 1 e shows a Ni grain with WC nanoparticles on its surface, and Fig. 1f shows the corresponding composition map before mixing with Al powders. Finally, Al powder was added and the final preparation of the mixture of powders was done in a mixer for 02 h at 12 RPM.

Powder mixtures with and without carbide particles were deposited by plasma transferred arc (PTA) on stainless steel plates of AISI 304 (150 mm  $\times$  100 mm  $\times$  10 mm). A total of 100-mm length single-layer coatings were deposited in a preheated substrate at 200 °C to better control the cooling rate and avoid cracks. Deposition current of 100 A and 120 A were used for all three powder mixture compositions. All other parameters were kept constant (Table 2).

**Fig. 1** **a** Ni particle; **b** Al particles; **c** WC–Co microparticles; **d** WC nanoparticles; **e** Ni particle with WC NPs on its surface; **f** composition map of Ni grain with NPs on its surface

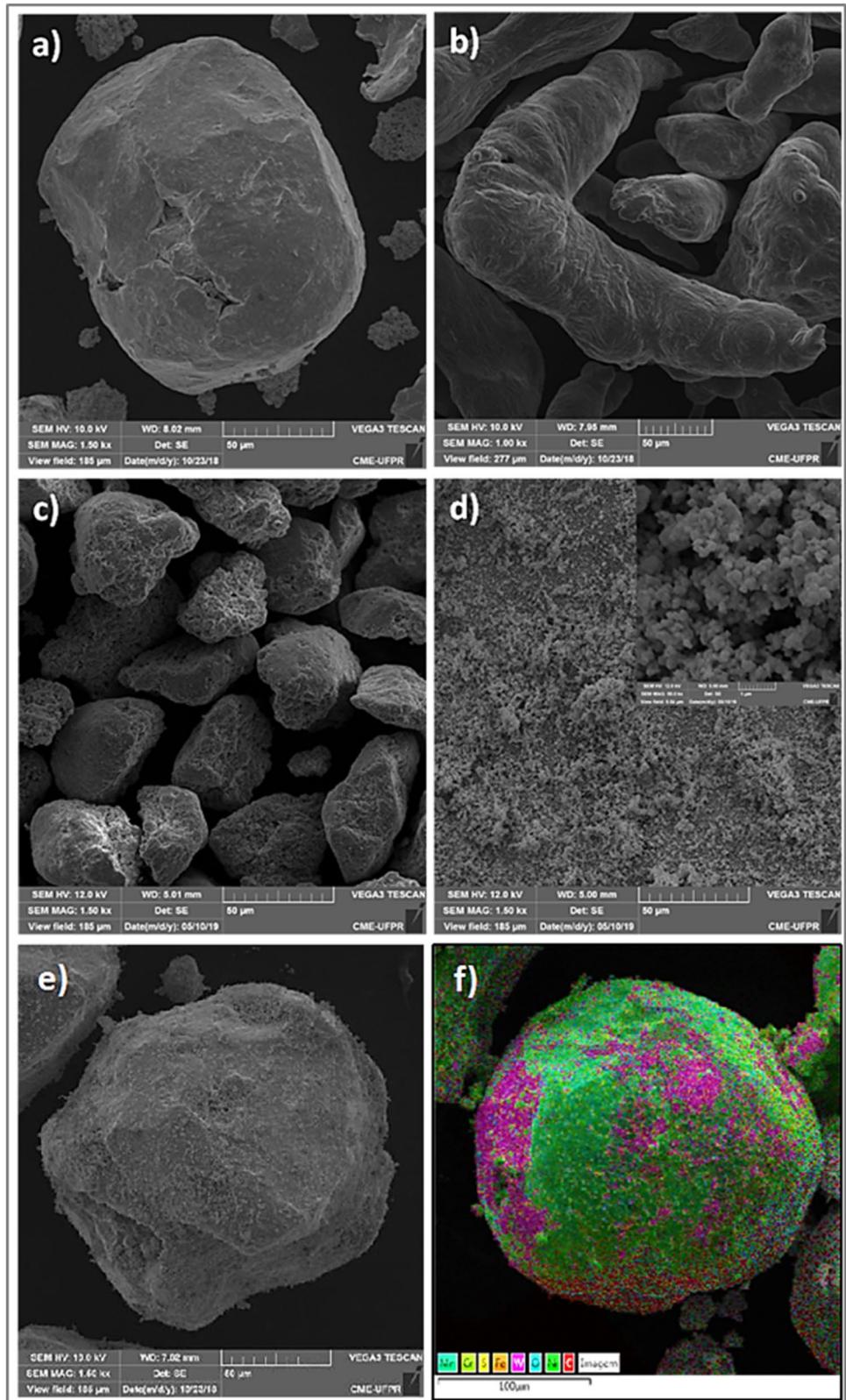


**Table 1** Composition of powder mixtures used for the coatings

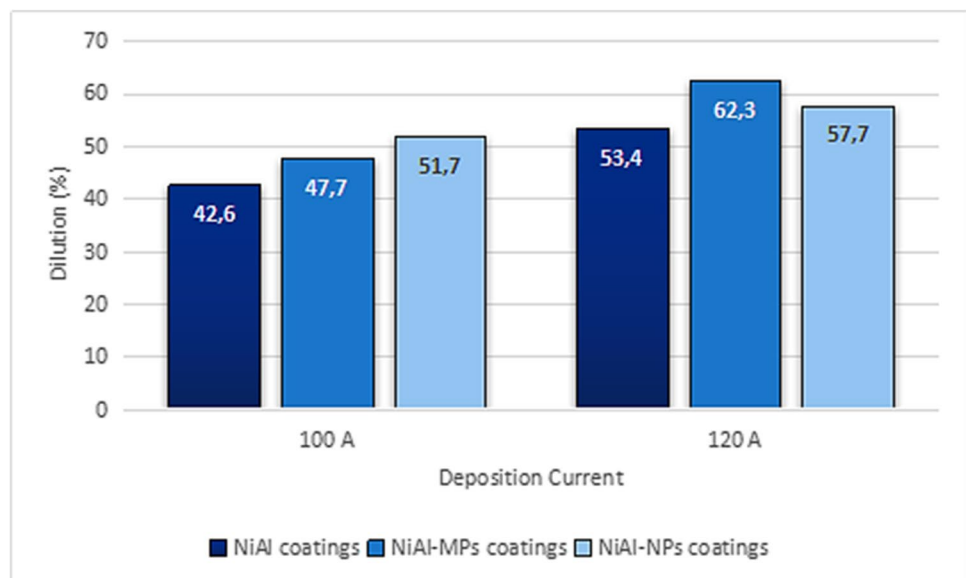
Powder mixture	Composition
Ni + Al	80 wt% Ni + 20 wt% Al
NiAl-MPs	Ni + Al mixture + 1 wt% WC–Co (MPs)
NiAl-NPs	Ni + Al mixture + 1 wt% WC (NPs)

**Table 2** Processing parameters

Plasma gas flow	2.0	l/min
Gas flow protection	15.0	l/min
Powder flow gas	1.0	l/min
Powder feed rate	6.0	g/min
Torch distance	10	mm
Deposition current	100, 120	A
Deposition speed	100	mm/min

Deep dye testing was used to detect cracks emerging at the surface of coatings. To better assess the impact of carbide particle size in NiAl in situ synthesis, using a fixed set of processing, a comparative analysis of the coatings for each deposition current was conducted. Coatings were characterized for their microstructure (morphology and phases), dilution with the substrate (chemical analysis), and hardness (Vickers Hardness) measured at the cross-section of the coatings.

X-ray diffraction analysis was performed on the top surface to identify the phases in the coatings, using Cu  $\alpha$  radiation ( $\lambda = 0.15406$  nm), scan of 1.0 degrees/min from 30 to 120°. The upper surfaces of the coatings were ground (up to 1200 grit sandpaper) and polished with alumina polishing suspension (1  $\mu$ m) before analysis.

**Fig. 2** Dilution of the coatings assessed by the Fe ratio (Eq. (1))

The microstructure was analyzed using scanning electron microscopy (SEM) and laser confocal microscopy on the cross-section of the coatings, ground and polished (final polishing with alumina 1  $\mu$ m) following standard metallographic procedures.

The dilution of the coating with the substrate steel was assessed by the iron content incorporated in coatings. This is done by a chemical method chosen when the geometry of the molten zone is irregular [11]. This procedure refers to the ratio between the variation in Fe content due to deposition ( $Fe_{\text{coating}} - Fe_{\text{powder mixture}}$ ) and iron content in the substrate,  $Fe_{\text{substrate}}$  (Eq. 1). The composition of coatings, including  $Fe_{\text{coating}}$ , was determined at the cross-section of the coatings, using energy-dispersive spectroscopy (EDS), over an area of 80 mm<sup>2</sup> with a DSS detector, coupled to the scanning electron microscope.

$$\text{Dilution (\%)} = \frac{Fe_{\text{coating}} - Fe_{\text{powder mixture}}}{Fe_{\text{substrate}}} \quad (1)$$

Microhardness tests were performed with a HMV-2 T Shimadzu microhardness tester with a Vickers penetrator and a normal force of 0.3 kgf to obtain the hardness profile of the coatings at the transverse cross-section (average of 3 profiles). The vertical spacing between indentations was 200  $\mu$ m, starting at the coating surface.

### 3 Results and discussion

Sound and crack-free coatings were obtained for all processed compositions and deposition current tested, as confirmed by deep dye testing. The dilution of coatings with the substrate (Fig. 2) determined according to Eq. 1



shows an increase with the deposition current from 100 to 120 A. This is an expected behavior when hardfacing superalloys or iron-based alloys as an increment in the heat input occurs with increasing deposition current melting a larger volume of substrate [15]. However, it is relevant to comment on the high dilution measured in the processed single-layer coatings that varied within the range 42.6 to 62.3%. It has been mentioned in the literature that when processing aluminides by in situ synthesis during the deposition of powder mixtures high dilution with the substrate occurs. This result can be accounted for by several factors, in particular, low thermal conductivity ( $K_{500^{\circ}\text{C}} = 21.5 \text{ W (m}\cdot\text{k)}^{-1}$ ) of the AISI 304 stainless steel substrates [15] that concentrates heat in the melt pool and heat-affected zone; the large negative heat of formation of the aluminide compounds ( $-72.0 \text{ kJ/mol}$  for NiAl and  $-36.6$  for  $\text{Ni}_3\text{Al}$ ), which means that large amounts of heat are release at the solidification front [5]; and the narrow solidification range of aluminides reducing liquid movements in the melt pool before solidification [7].

The addition of 1 wt% of microparticles (NiAl-MP coatings) and nanoparticles (NiAl-NP coatings) to the Ni–Al powder mixture further increased dilution compared to that of coatings processed with Ni + Al powder mixtures. Previous work reported an increase in the dilution of Co-based alloy coatings after adding a much larger amount of WC–Co particles (35 wt%) to an atomized Co-based alloy. This behavior was associated with the low thermal conductivity of carbides and the energy that is retained in these particles as they cross the plasma arc, which is released by conduction and radiation in the melt pool. A similar effect to that expected when increasing the heat input [14].

The increase in dilution following the modification of Ni + Al powder mixtures with WC nanoparticles agrees with data reported for coatings processed with Ni superalloys modified with nanoparticles that reported an increase in dilution [13]. Authors associated the increase in dilution with high reactivity via the exothermic reactions of WC NPs that increase the temperature of the melt pool, hence the liquid movements in the melt pool.

In situ synthesis of aluminides during the deposition of Ni + Al-based powder mixture is confirmed by X-ray diffraction analysis at the surface of the coatings (Fig. 3). The presence of aluminides and the austenitic Fe–Ni phase is in agreement with data reported by Brunetti et al. [11] that processed Ni + Al powder mixtures on carbon steel substrates. Also, according to Fe–Ni–Al ternary phase diagram [16], the ordered  $\beta$ -NiAl is expected, together with the austenitic phase for the range of composition of the processed coatings. Almeida et al. [7] in their study of NiAl coatings report that for compositions with iron content above 25 at.% Fe, the presence of  $\gamma$ -FeNi is expected. In spite of the Fe availability during processing,

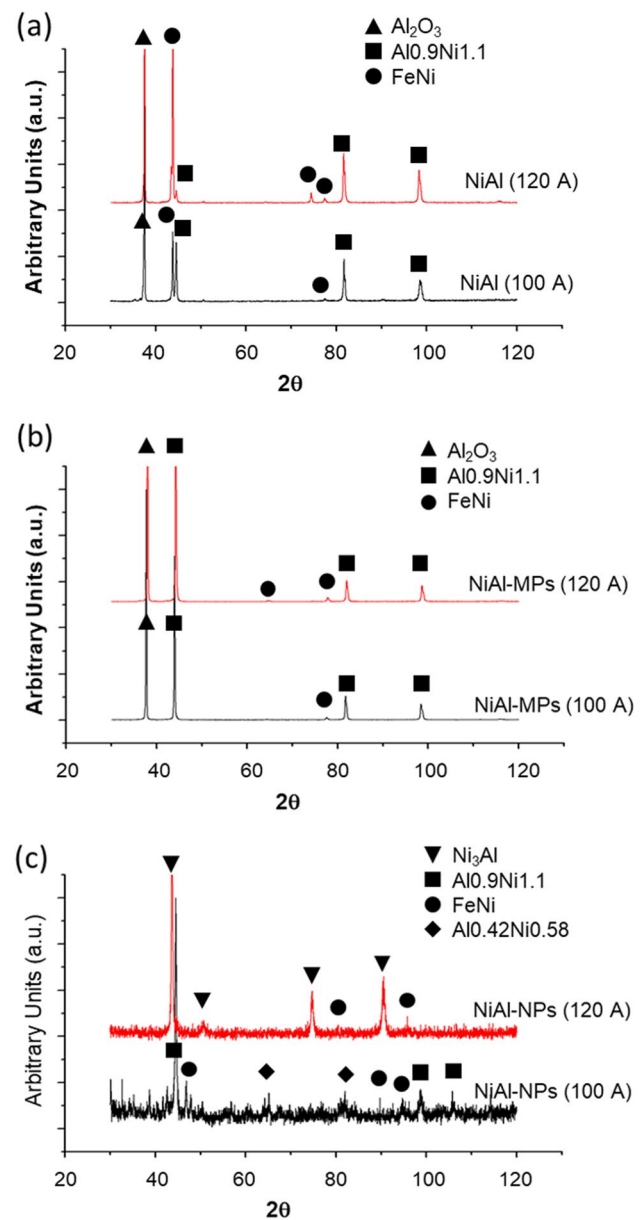


**Fig. 3** XRD of the processed coatings. **a** NiAl; **b** NiAl+MPs, **c** NiAl+NPs

Fe aluminides were not identified in the coatings. Brunetti and co-authors [11] associated this behavior with the higher enthalpy of formation of Fe aluminides compared with NiAl enthalpy of formation ( $-72 \text{ kJ/mol}$  for NiAl versus  $-26.5 \text{ kJ/mol}$  for FeAl).

A detailed analysis of the aluminide compounds formed in coatings (Fig. 4) reveals that the powder mixture composition impacts the characteristics of the ordered compounds that constitute each coating. The  $\gamma$ -FeNi austenitic phase together with aluminide compounds is present in all coatings. Processing Ni + Al powder mixtures leads to the synthesis of  $\beta$ -NiAl (Ni<sub>1.1</sub>Al<sub>0.9</sub>), with a peak shift

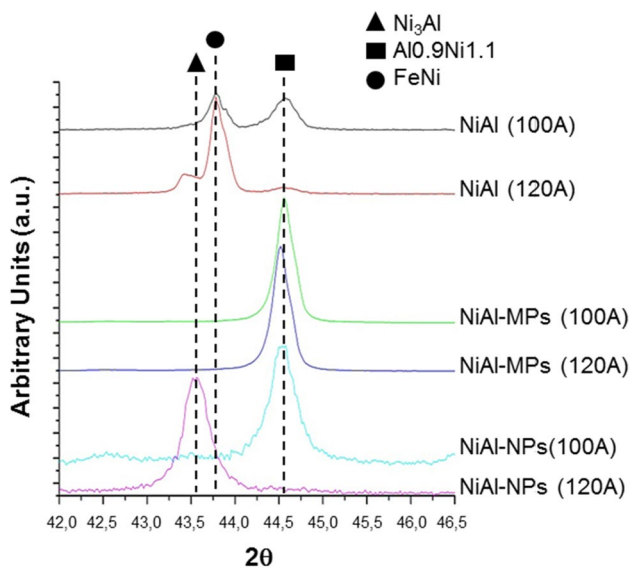


**Fig. 4** Detailed analysis of the main XRD peak of the processed coatings

from  $2\theta = 44.50$  to  $44.54^\circ$  with increasing deposition current. The peak shift can be associated with the increasing Fe content as measured by dilution. The same compound,  $\beta$ -NiAl ( $\text{Ni}_{1.1}\text{Al}_{0.9}$ ), forms when WC-Co MPs were added to the Ni + Al powder mixture (with a peak shift from  $2\theta = 44.56$  to  $44.52^\circ$  with increasing current). The dissolution of carbides makes alloying elements available that have solubility in both FeNi austenitic phase and NiAl. Almeida et al. [7] mentioned the high solubility of Co in NiAl, and literature shows that the solubility limit of W in NiAl ( $\text{Ni}/\text{Al} = 1$ ) ranges from 0.4 to 1 at.% [17, 18]. These results are consistent with those reported by Yuan et al. [8] that processed NiAl/WC composites through thermal explosion reaction from Ni, Al, and WC (25–40  $\mu\text{m}$ ) elementary powders, obtaining the complete synthesis of  $\beta$ -NiAl phase for mixtures containing 3 to 5 wt% WC. However, the presence of WC (NPs) interferes with the in situ synthesis of the aluminide, making the synthesis of ordered compound more dependent on the deposition current. Coatings processed with 100 A exhibit NiAl,  $\text{Al}_{0.9}\text{Ni}_{1.1}$  ( $2\theta = 44.58^\circ$ ) together with richer Ni aluminide  $\text{Al}_{0.42}\text{Ni}_{0.58}$ . The increase in the deposition current to 120 A results in the synthesis of  $\text{Ni}_3\text{Al}$  ( $2\theta = 43.56^\circ$ ) without the NiAl aluminide.

A better understanding of the synthesis occurring in coatings processed with different powder mixtures was gained from EDS semiquantitative chemical analysis at the cross-section of deposits. Table 3 shows the Ni/Al (at.%) ratio measured for each processed coating for each powder mixture and deposition current used. Also included is the equilibrium Ni/Al ratio (at.%). According to the Ni–Al phase

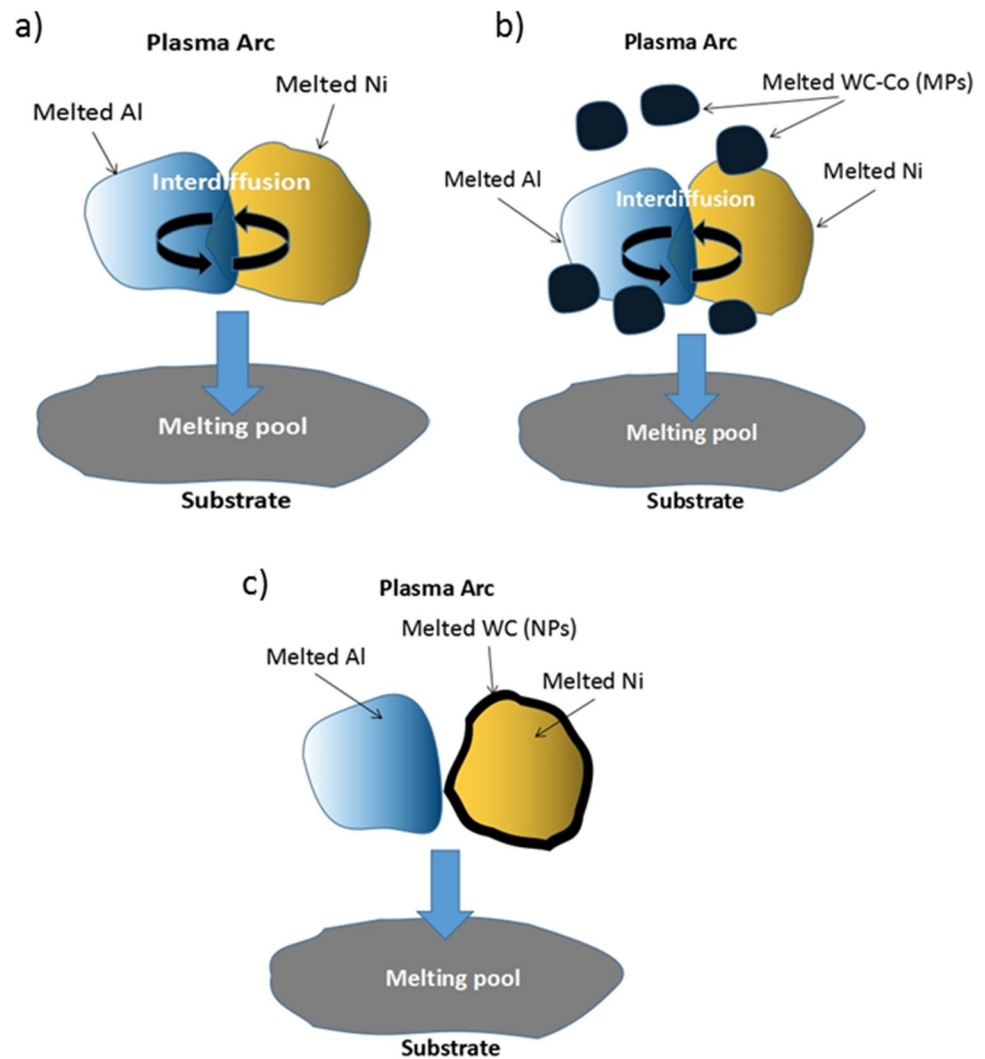
**Table 3** Ni/Al ratio measured in the processed coatings

Coating	Ni/Al (at.%/ at.)	
	100 A	120 A
NiAl	1.9	2.0
NiAl-MPs	1.5	1.7
NiAl-NPs	2.2	3.1
<b>Equilibrium Ni/Al:</b>	0.74–2.24	

diagram [19], the solubility limit of  $\beta$ -NiAl varies between 42.85 at.% Ni and 69.17 at.% Ni, resulting in Ni/Al ratios ranging from 0.74 to 2.24.

Analysis of Ni/Al ratio data reveals that coatings processed with Ni + Al and (Ni + Al)-MP powder mixtures exhibit Ni/Al ratios within the range offered by the equilibrium  $\beta$ -NiAl compound. However, a higher Ni/Al ratio was measured on coatings processed with the powder mixture modified with WC nanoparticles (NiAl-NPs), 2.2 and 3.1 for 100 and 120 A, respectively. According to Ni–Al phase diagram, these values are typical for Ni-rich aluminides, in agreement with the formation of Ni-rich phases such as  $\text{Al}_{0.42}\text{Ni}_{0.58}$  or  $\text{Ni}_3\text{Al}$ . This analysis raises the hypothesis that the interaction between Ni and Al in the plasma arc and melt pool is compromised. Further understanding was gained from investigating the behavior of powders as each mixture crosses the plasma arc (Fig. 5). The work of Almeida et al. [7] on in situ synthesis of NiAl corroborated that the synthesis of the aluminide compound starts with the interaction between droplets of Ni and Al in the plasma arc (Fig. 5a). The interaction in the plasma arc is expected as interdiffusion is very fast in the liquid phase [20]. The synthesis continues in the substrate once the melted powders reach the melt pool, where alloying elements are incorporated in the Ni aluminide. This scenario does not change with the addition of WC-Co (MPs) (Fig. 5b). Powder particles from each material melt in the plasma arc, and the melted WC-Co droplets neither delayed nor inhibit the interdiffusion between Ni and Al, the elements being incorporated in the coatings as solid solution strengtheners.

The powder mixtures containing nanoparticles respond differently to the energy of the plasma arc, nanoparticles adherent on the surface of Ni powder grains melt forming a liquid film around Ni particles (Fig. 4c). Although WC melting point is  $2870^\circ\text{C}$ , WC nanoparticles have a considerably lower melting point than bulk material, resulting in a droplet of a bi-material. The liquid WC film behaves as a barrier to the interdiffusion of Ni and Al, which is necessary to form NiAl, leaving elementary powders exposed to the plasma arc. As the droplets reach the melt pool, the liquid film breaks but the competition between the synthesis of aluminides and austenite favors the latter.

**Fig. 5** Schematic representation of powders in the plasma arc

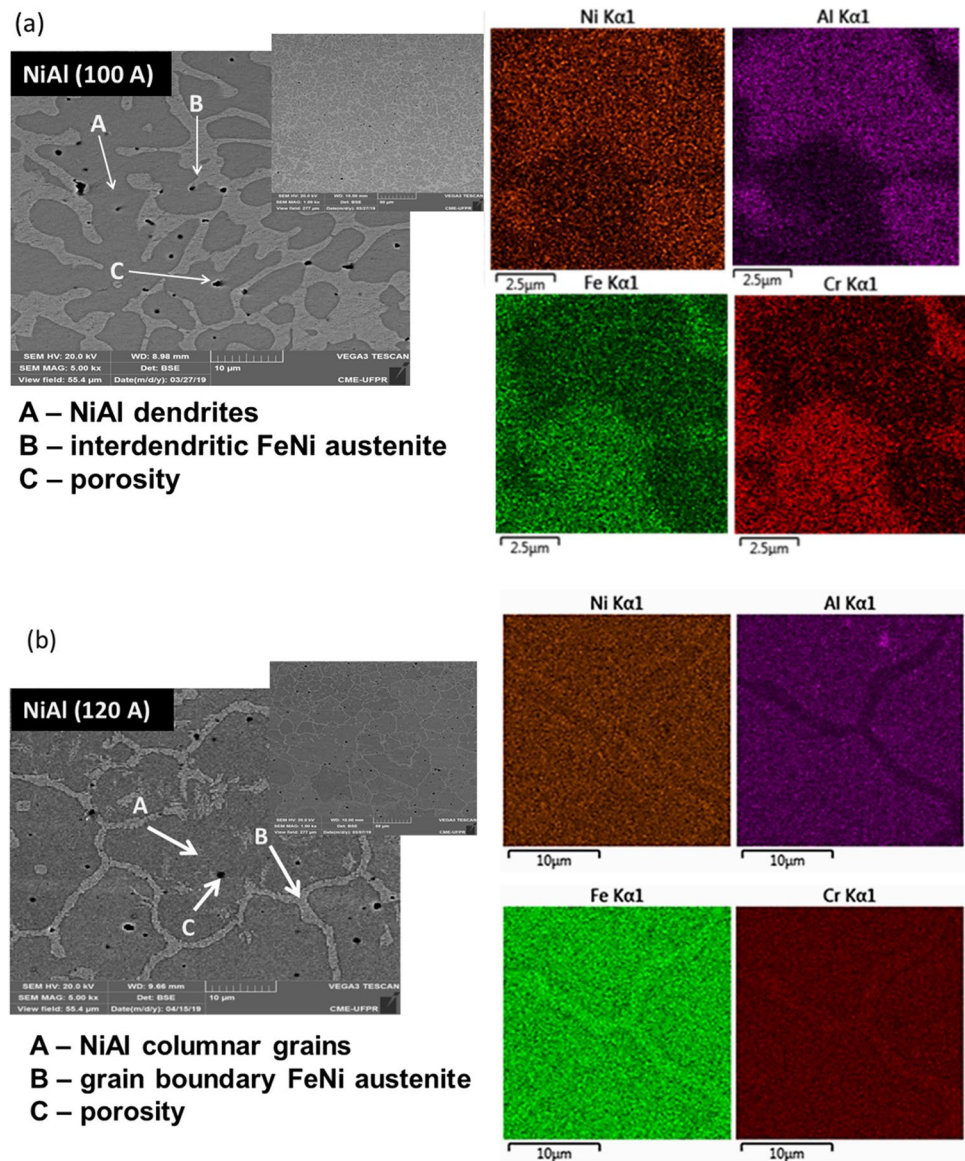
During the deposition of powder mixtures containing NPs, it is also relevant to consider that as Al does not bond to Ni in the plasma arc, this lighter, lower melting point (Al melting point is  $\sim 660$  °C; Ni melting point is 1455 °C) and lower heat of vaporization element in the mixture (Al heat of vaporization is  $\sim 284$  kJ/mol; Ni heat of vaporization is  $\sim 379$  kJ/mol) vaporize leading to more significant losses of Al. Hence, the reduced Al availability in the melt pool, that further increases the Ni/Al ratio, also induces the synthesis of richer Ni compounds ( $\text{Al}_{0.42}\text{Ni}_{0.58}$  and  $\text{Ni}_3\text{Al}$ ) and the higher Ni available favors the formation of the austenitic FeNi phase.

The loss of elements is expected during elementary powder deposition by PTA, and it becomes more significant for lighter, low melting point elements, such as aluminum [7]. These authors reported aluminum losses of up to 28% when depositing Ni–Al coatings from elementary powders, changing considerably the initial composition.

To further test the hypothesis of the behavior of powders during deposition, it is of relevance to investigate the microstructure of coatings processed with the different powder mixtures.  $\beta$ -NiAl dendritic solidification structures with interdendritic the  $\gamma$ -FeNi austenitic phase form in coatings processed with the Ni + Al powder mixture, regardless of the deposition current used (Fig. 6). The microstructure of coatings is consistent with the reports by Benegra et al. [21] that processed Ni + Al powder mixtures containing Cr and carbides. The higher interaction with the substrate of coatings processed with 120 A (higher dilution) accounts for the larger fraction of  $\gamma$ -FeNi austenitic phase at the interdendritic region (Fig. 6b), as supported by chemical composition maps for Fe and Cr. Spherical porosity observed in the microstructure is associated with the exothermal reaction and irregular porosity with unmelted powder particles.

Coatings were processed with the (Ni + Al) powder mixtures with microparticles (NiAl-MPs coatings); Fig. 7

**Fig. 6** Microstructure and composition maps of coatings processed with the NiAl powder mixture **a** 100A and **b** 120A



a and b exhibit a distribution of the elements similar to that of coatings without the carbide particles (NiAl coatings): Columnar  $\beta$ -NiAl solidification structures with Fe and Cr segregated at grain boundaries in the thin layer of the austenite phase, whereas deposition with 120 A resulted in a dispersion of an acicular phase within the NiAl grains. Porosity is also present in coatings.

Different phase distribution is found in coatings processed with (Ni + Al) powder mixture modified with nanoparticles (NiAl-NP coatings), a consequence of the powder mixture preparation and behavior of particles as they cross the plasma arc (Fig. 8 a and b). Regardless of the deposition current used,  $\gamma$ -FeNi austenitic dendritic structure with interdendritic Ni-rich aluminides ( $Al_{0.42}Ni_{0.58}$  and  $Ni_3Al$ ) formed, this is a consequence of the restrained interaction between

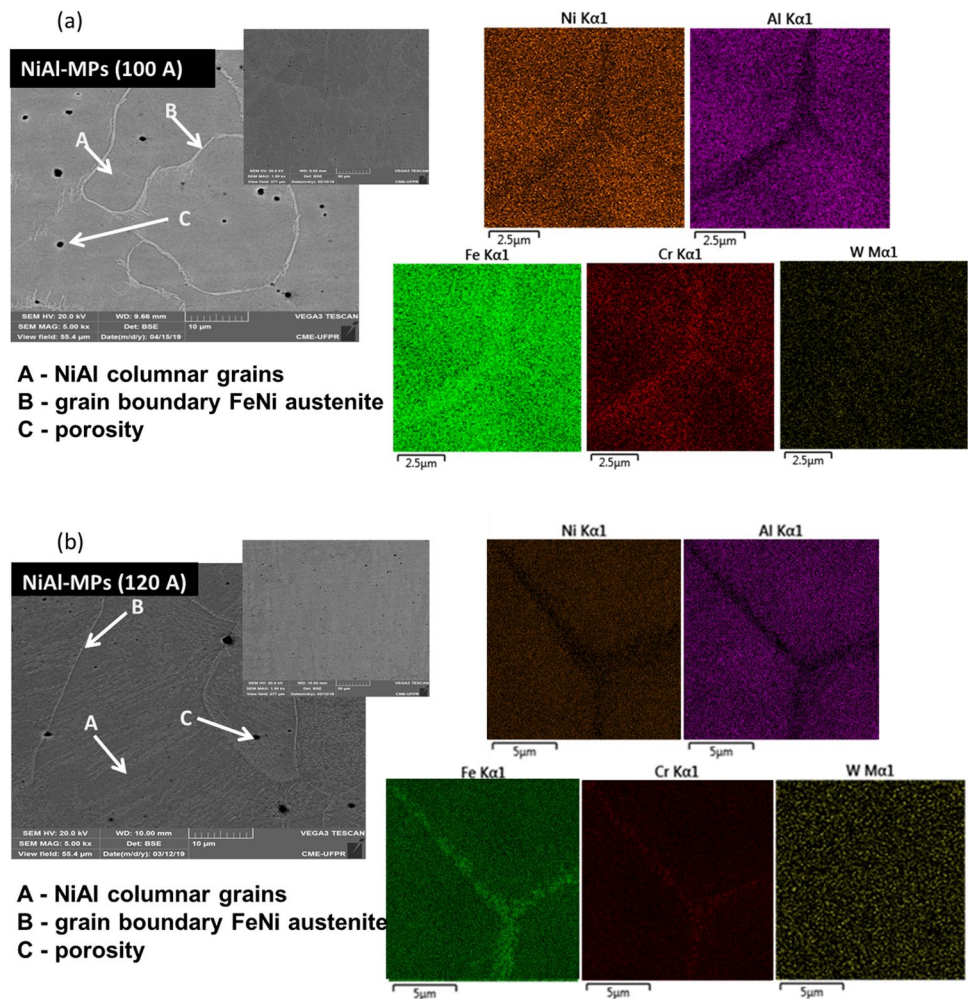
Ni and Al due to the molten WC film surrounding the Ni particles.

The observed interference in the synthesis of NiAl is considerably different behavior from that exhibited by superalloys modified with ceramic nanoparticles (such as WC,  $ZrO_2$  and  $TiO_2$ ) that showed grain refinement induced by NPs, which has been associated with Zener Pinning mechanisms [13, 22, 23].

The liquid film around the Ni particles caused by the melting nanoparticles is a barrier to the interaction between Ni and Al in the plasma arc compromising the in situ synthesis of the  $\beta$ -NiAl compound in coatings; under these conditions, it is not possible to establish a direct comparison on the contribution of microsized and nanosized particles on the mechanical properties of the coatings. It is necessary



**Fig. 7** Microstructure and composition maps of NiAl-MP coatings processed with **a**100A and **b**120A



to explore routes to prepare powder mixtures with nanoparticles that allow prevent nanoparticles agglomeration but allow required interaction between elements for the in situ synthesis of  $\beta$ -NiAl to occur.

The preponderance of the  $\gamma$ -FeNi austenitic phase in coatings processed with powder mixtures containing NPs impacts hardness profiles (Fig. 9). An average hardness of  $264.3 \pm 11$  HV and  $193.6 \pm 12$  HV was measured for coatings processed with 100 A and 120 A, respectively, a small increase to that of the substrate steel hardness (150–200 HV).

In contrast, hardness of aluminide coatings, processed both with Ni + Al and (Ni + Al)-MP powder mixtures increases with deposition current hence dilution: NiAl coatings processed with the Ni + Al powder mixture, exhibited an increase on hardness from  $365.2 \pm 12$  HV to  $406.3 \pm 10$  HV when processing with 100 A and 120 A, respectively (Fig. 9). These results are consistent with the trend reported by Brunetti et al. [11] in their discussion of the impact of Fe in point defect density in NiAl coatings hardness. These authors claimed that an increase in deposition current from

100 to 120 A lead to an increase on average hardness of approximately 6%, which was related to solid solution strengthening with Fe [24] and Cr [25]. The average hardness of NiAl-MP coatings was similar for coatings processed with both 100 A and 120 A,  $490.8 \pm 13$  HV, and  $485.6 \pm 12$  HV, respectively. The higher measured hardness compared to that of coatings processed with Ni + Al powder mixtures (Fig. 9) is a consequence of higher alloying element content from the substrate (higher dilution) together with the alloying elements from melted carbide.

The solid solution strengthening of NiAl depends on the density and type of point defects formed. This behavior is a consequence of the sublattice each alloying element occupies, although a few elements, such as Fe, can occupy both Ni and Al sublattices [26]. Constitutional defects that are present in non-stoichiometric NiAl are vacancies (Al-rich compositions) and anti-sites (Ni-rich compositions). Vacancies have a stronger hardening effect than anti-sites and the addition of Fe impacts both of these defects depending on the stoichiometry of NiAl compound. The concentration of each of these defects impacts hardness

**Fig. 8** Microstructure of NiAl-NP coatings and composition maps. Processed with **a** 100A and **b** 120A

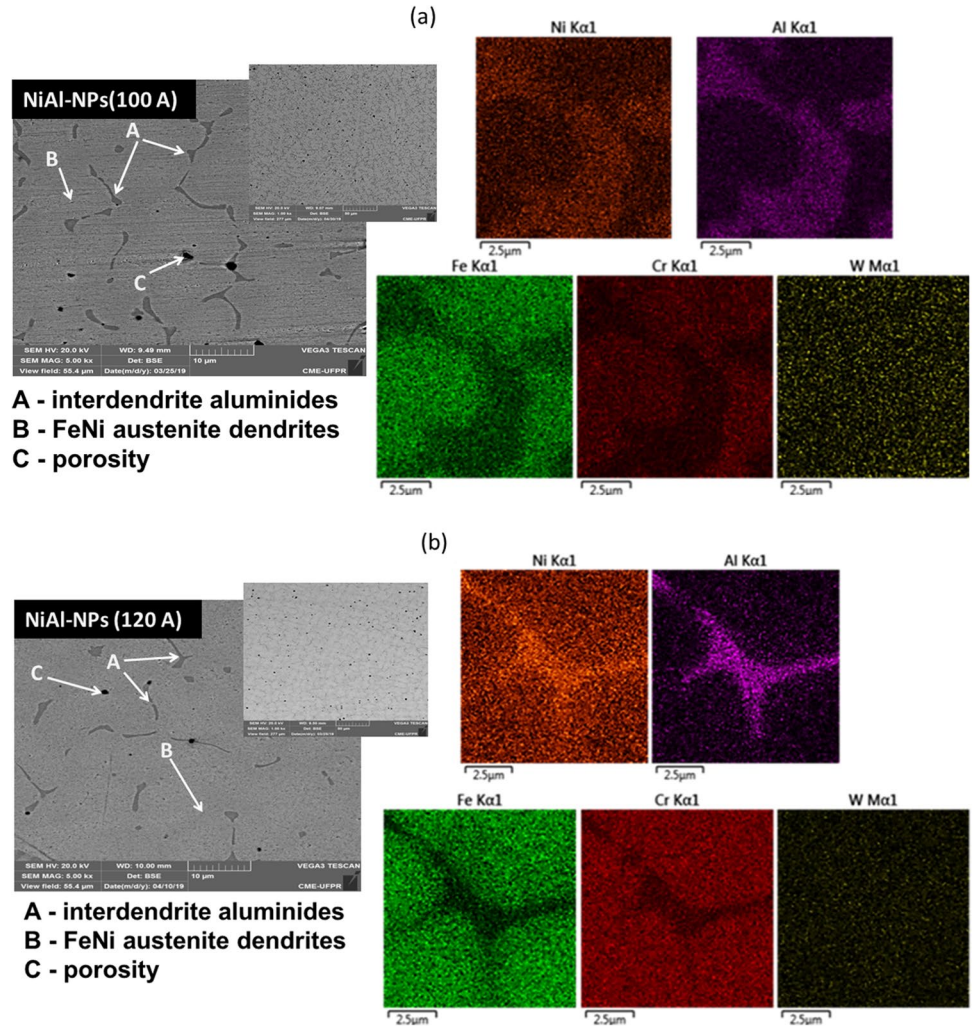
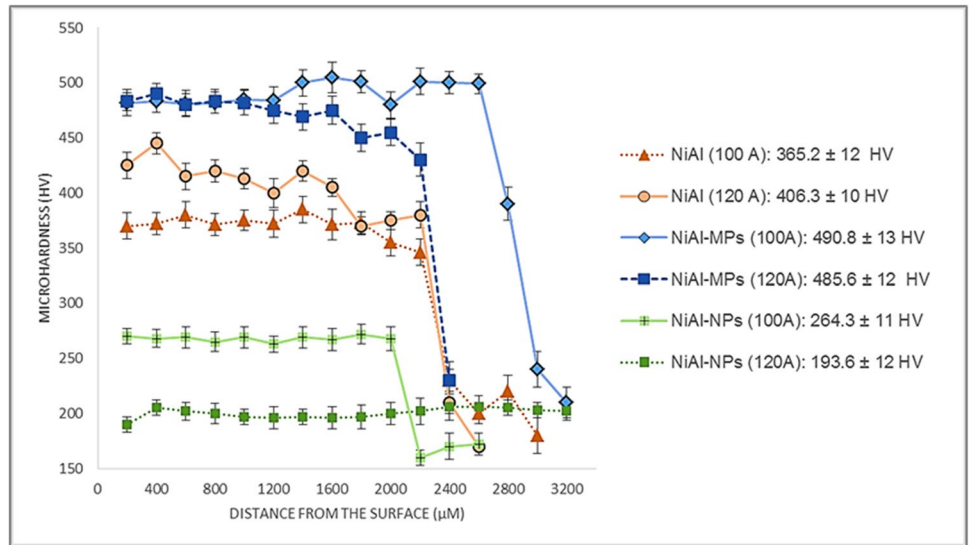


**Fig. 9** Microhardness Vickers (0.3 kgf) of the transversal section of the coatings and average hardness (HV)



differently [26]. Brunetti et al. [11] assess the impact of Fe in NiAl coatings for Fe content in the range between 14 and 43 at.%. These authors claim that Ni anti-sites form for low Fe content with little hardening effect, and that further increase in Fe content led to a considerable increase in hardness associated with vacancies together with anti-sites in the Ni sublattice.

Extrapolating the theory put forward by Brunetti et al. [11], to the processing conditions used in the present study of the impact of different alloying elements in NiAl coating hardness, the increase in hardness can be associated with the observed increase in dilution and the consequent creation of vacancies in the Ni sublattice.

Besides Fe, the effect of Cr diffusing from the substrate into NiAl coating must also be considered. Cr can substitute Ni or Al in the ordered structure, the formation of Ni vacancies and anti-sites accounting for the solid solution hardening of Cr in NiAl [22]. NiAl alloys containing Cr as a ternary element form a pseudo-binary eutectic NiAl-CCC system in which the solubility of Cr in NiAl is very limited. For Ni/Al = 1, at room temperature, the maximum solubility of Cr is nearly 1 at.% and goes up to about 10 at.% near to eutectic temperature. Al content can also affect the solubility, with the B2 phase dissolving more Cr as Al content decrease, which implies that Cr has a preference for the Al sublattice [25]. These authors also affirm that NiAl alloys with Cr content above 1 at.% showed an increase in hardness because of the presence of constitutional anti-sites or vacancies. Extrapolating these findings to the present study allows to associate the increasing NiAl coating hardness with deposition current with a higher Cr diffusing from the substrate being incorporated in the ordered structure of coatings.

The contribution of Fe and Cr to the increase of hardness in NiAl aluminide is also observed in the coatings containing MPs (NiAl-MP coatings). Nevertheless, the addition of MPs has a two-fold impact in the density of point defects: the mentioned increase in dilution that allows for more Fe and Cr to diffuse from the substrate and the impact W, C, and Co from the melted carbide particles. Although the quantities of these elements added to the melt pool is low, so is the solubility of W and C in the ordered NiAl. The former is reported to exhibit a solubility that varies between 0.04 and 1 at.% [17, 18]. Also, C has demonstrated to be a very potent strengthening element in NiAl > 1700 MPa/at.% [27]. Similarities between Co and Ni make the substitution in the Ni sublattice favorable. In summary, a higher density of point defects in NiAl ordered structure is expected as a consequence of the presence of WC-Co particles in the deposited powder mixture, accounting for the increase in the average hardness of coatings.

## 4 Conclusions

Under the conditions used in this research of the effect of micro (WC-Co) and nano (WC) particles in the in situ synthesis of aluminide coatings during the PTA deposition of Ni + Al elemental powder mixtures, it is possible to conclude the following:

1. The synthesis of the  $\beta$ -NiAl aluminide occurs during deposition of Ni + Al powder mixtures on the stainless steel substrate; the solidification structure exhibits an increase in the hardness with the density of point defect in the ordered lattice, induced by dilution with the substrate.
2. The deposition of Ni + Al elemental powder mixtures containing WC-Co microparticles resulted in harder  $\beta$ -NiAl columnar structure coatings, accounted for solid solution hardening, a consequence of the presence of more alloying elements contributing to an increase in point defect density in the aluminide lattice.
3. The synthesis of  $\beta$ -NiAl in coatings was compromised when nanoparticles were added to the Ni + Al powder mixtures. This is a consequence of the WC-NPs forming a liquid film surrounding the Ni grain particles that interfere in the interdiffusion of Ni and Al during deposition favoring the formation of a low hardness  $\gamma$ -FeNi austenitic dendrite microstructure as oppose to  $\beta$ -NiAl solidification microstructure.

**Acknowledgements** Important contributions were also gained from the use of equipment from the Electron Microscopy Center—CME/UFPR, X ray diffraction facilities, and Laboratory of Additive Manufacturing and Surface Engineering – LAMSE/UFPR.

**Author contribution** - H. O Abreu-Castillo — Methodology, Investigation, Data Curation, Writing—Original Draft, Writing—Review & Editing, Visualization.

- B. P. Bueno — Methodology, Investigation, Data Curation.

- Ana Sofia C. M. d'Oliveira — Conceptualization; Methodology, Investigation, Resources, Writing—Review & Editing, Supervision, Project administration, Funding acquisition.

**Funding** This work was supported by Coodenação de aperfeiçoamento de pessoal de nível superior — CAPES and Fundação Araucária/PR for the scholarship of Mr Abreu Castillo and CNPq — Conselho Nacional de Desenvolvimento científico e tecnológico (Grant # 3096608/2019–8).

**Availability of data and material** Available upon request as this is parts.

**Code availability** Not applicable.

## Declarations

**Ethics approval** This is an original work that has not been published or considered for publication elsewhere in any form or language.



**Consent to participate** Not applicable.

**Consent for publication** Not applicable.

**Conflict of interest** The authors declare no competing interests.

## References

- Ozdemir O, Zeytin S, Bindal C (2010) Characterization of NiAl with cobalt produced by combustion synthesis. *J Alloy Compd* 508(1):216–221. <https://doi.org/10.1016/j.jallcom.2010.08.056>
- Miracle DB, Darolia R (2000) NiAl and its Alloys. In: Westbrook JH, Fleischer RL (eds) *Intermetallic compounds: structural applications of intermetallic compounds*, vol 3. Wiley, Inglaterra, pp 55–74
- Meetham GW, Van De Voorde MH (2000) *Materials for high temperature engineering applications*. Springer, Berlin
- Yan K, Guo H, Gong S (2014) High-temperature oxidation behavior of  $\beta$ -NiAl with various reactive element dopants in dry and humid atmospheres. *Corros Sci* 83:335–342. <https://doi.org/10.1016/j.corsci.2014.02.033>
- Noebe RD, Bowman RR, Nathal MV (1996) The physical and mechanical metallurgy of NiAl. In: Stoloff NS, Sikka VK (eds) *Physical metallurgy and processing of intermetallic compounds*. Chapman & Hall, New York, pp 212–296
- Shokati AA, Parvin N, Sabzianpour N, Shokati M, Hemmati A (2013) In situ synthesis of NiAl–NbB<sub>2</sub> composite powder through combustion synthesis. *J Alloy Compd* 549:141–146. <https://doi.org/10.1016/j.jallcom.2012.08.024>
- Almeida VB, Takano EH, Mazzaro I, d’Oliveira ASCM (2011) Evaluation of Ni–Al coatings processed by plasma transferred arc. *Surf Eng* 27(4):266–271. <https://doi.org/10.1179/026708410X12550773057866>
- Yuan J, Zhang X, Zhang C, Sun K, Liu C (2016) In-situ synthesis of NiAl/WC composites by thermal explosion reaction. *Ceram Int* 42(9):10992–10996. <https://doi.org/10.1016/j.ceramint.2016.03.237>
- Miracle DB, Mendiratta MG (2000) Intermetallic composites. In: Westbrook JH, Fleischer RL (eds) *Intermetallic compounds: structural applications of intermetallic compounds*, vol 3. Wiley, Inglaterra, pp 293–307
- Deuis RL, Yellup JM, Subramanian C (1998) Metal-matrix composite coatings by PTA surfacing. *Compos Sci Technol* 58(2):299–309. [https://doi.org/10.1016/S0266-3538\(97\)00131-0](https://doi.org/10.1016/S0266-3538(97)00131-0)
- Brunetti C, Pintaude G, d’Oliveira ASCM (2014) The influence of Fe content on the mechanical properties of NiAl coatings processed in situ. *J Mater Eng Perform* 23(11):3934–3940. <https://doi.org/10.1007/s11665-014-1203-5>
- He F (2013) Ceramic nanoparticles in metal matrix composites. In *Ceramic nanocomposites*. Woodhead Publishing, pp 185–207. <https://doi.org/10.1533/9780857093493.2.185>
- Molina-Claros J, Hdz-García HM, Alvarez-Vera M, Pech-Canul MI, Muñoz-Arroyo R, García-Vázquez F, Díaz-Guillen JC (2017) Characterisation of PTA processed overlays without and with WC nanoparticles. *Surf Eng* 33(11):857–865. <https://doi.org/10.1080/02670844.2017.1323442>
- D’Oliveira ASCM, Tigrinho JJ, Takeyama RR (2008) Coatings enrichment by carbide dissolution. *Surf Coat Technol* 202(19):4660–4665. <https://doi.org/10.1016/j.surfcoat.2008.03.034>
- Yaedu AE, D’oliveira ASCM (2005) Cobalt based alloy PTA hardfacing on different substrate steels. *Mater Sci Technol* 21(4):459–466. <https://doi.org/10.1179/174328413X13789824293380>
- Raynor GV, Rivlin VG (1988) *Phase equilibria in iron ternary alloys: a critical assessment of the experimental literature*. The Institute of Metals, 1 Carlton House Terrace, London
- Milenkovic S, Schneider A, Frommeyer G (2011) Constitutional and microstructural investigation of the pseudobinary NiAl–W system. *Intermetallics* 19(3):342–349. <https://doi.org/10.1016/j.intermet.2010.10.019>
- Alekseeva ZM (1993) Al–Ni–W (aluminium–nickel–tungsten). MSIT Ternary Evaluation Program, in MSIT Workplace
- Nash P, Singleton MF, Murray JL (1992) Al–Ni phase diagram. In: ASM metals handbook. Alloy phase diagrams, vol 3, p 311
- German RM, Iacocca RG (1996) *Powder metallurgy processing*. In: Stoloff NS, Sikka VK (eds) *Physical metallurgy and processing of intermetallic compounds*. Chapman & Hall, New York, pp 605–654
- Benegra M, Pintaude G, D’Oliveira ASCM, Goldenstein H (2012) Characterization of NiCrAlC PTA coatings. *Mater Res* 15(5):775–778. <https://doi.org/10.1590/S1516-14392012005000098>
- Dabiri AR, Mojallal RY, Ahmadi E, Fattahi M, Amirkhanlou S, Fattahi Y (2015) Effect of ZrO<sub>2</sub> nanoparticles on the impact properties of shielded metal arc welds. *Mater Lett* 158:325–328. <https://doi.org/10.1016/j.matlet.2015.05.159>
- Ramkumar KR, Natarajan S (2018) Investigations on microstructure and mechanical properties of TiO<sub>2</sub> nanoparticles addition in Al 3003 alloy joints by gas tungsten arc welding. *Mater Sci Eng A* 727:51–60. <https://doi.org/10.1016/j.msea.2018.04.111>
- Munroe PR, George M, Baker I, Kennedy FE (2002) Microstructure, mechanical properties and wear of Ni–Al–Fe alloys. *Mater Sci Eng A* 325(1–2):1–8. [https://doi.org/10.1016/S0921-5093\(01\)01403-4](https://doi.org/10.1016/S0921-5093(01)01403-4)
- Cotton JD, Noebe RD, Kaufman MJ (1993) Ternary alloying effects in polycrystalline { $\beta$ }-NiAl (No. LA-UR-93–1395; CONF-930997–1). Los Alamos National Lab., NM (United States). <https://www.osti.gov/servlets/purl/10157276>
- Pike LM, Chang YA, Liu CT (1997) Solid-solution hardening and softening by Fe additions to NiAl. *Intermetallics* 5(8):601–608. [https://doi.org/10.1016/S0966-9795\(97\)00040-X](https://doi.org/10.1016/S0966-9795(97)00040-X)
- George EP, Liu CT (1990) Brittle fracture and grain boundary chemistry of microalloyed NiAl. *J Mater Res* 5(4):754–762. <https://doi.org/10.1557/JMR.1990.0754>

**Publisher's note** Springer Nature remains neutral with regard to jurisdictional claims in published maps and institutional affiliations.